Controlled Translational Manipulation of Small Latex Spheres by Dynamic Force Microscopy

Claudia Ritter,*,† Markus Heyde,†,‡ Udo D. Schwarz,‡,§ and Klaus Rademann†

Institute of Chemistry, Humboldt-University Berlin, Brook-Taylor Strasse 2, D-12489 Berlin, Germany, Lawrence Berkeley National Laboratory, Materials Sciences Division, University of California, 1 Cyclotron Road, Mailstop 66-200, Berkeley, California 94720, and Department of Mechanical Engineering, Yale University, 15 Prospect Street, New Haven, Connecticut 06520-8284

Received August 17, 2001. In Final Form: April 29, 2002

We report on the application of a home-built scanning force microscope for translation and in-plane rotation of nanometer-sized latex spheres by dynamic surface modification (DSM). This technique is based on the increment of the amplitude of the oscillating voltage applied at the dither piezo that drives the cantilever vibrations in the dynamic mode of scanning force microscopy. Thus, it is easily possible to switch between the imaging mode and DSM mode, enabling the direct manipulation of nanostructures under ambient conditions with high precision. The main advantage of our technique compared to earlier methods is that it operates with an active feedback loop, allowing a steady manipulation of nanostructures independent of the surface corrugation or sample tilt. Such controlled translations of latex spheres enable us in addition to study their properties regarding friction, adhesion, and cohesion. By translating latex spheres of different sizes (radii between 50 and 110 nm), it was found that the force needed to move a particle depends on its dimensions. Finally, the lateral translation of an intentionally marked sphere gives evidence that sliding is preferred over rolling.

1. Introduction

The use of a scanning force microscope (SFM) for surface modifications enables a large variety of new lithographic experiments on the nanometer scale.[1,2] For example, the sample surface can be directly patterned by the tip of an SFM. This can be carried out, for example, by scratching the surface with the SFM tip, called static plowing.[3,4] Alternatively, the surface can also be modified by indenting it with a vibrating tip, called dynamic plowing.[5−8]

With the same experimental setup as that used for dynamic plowing, small particles may be manipulated on the surface of a suitable substrate.[9,10] In this way, nanoparticles can be translated and in-plane rotated to form two-dimensional patterns from randomly arranged arrays of deposited particles on a given substrate. The corresponding experimental technique should be denoted as dynamic surface modification (DSM) in the following, comprising both the dynamic plowing technique, where local plastic deformation of the sample is induced, and the manipulation of structurally unchanged particles on a given substrate surface. As an additional benefit, a controlled sliding and dislocation of nanoparticles gives certain access to their frictional and adhesional properties that may contribute to a better understanding of the fundamental processes of friction.

Compared to the so-called contact mode, operation of an SFM in the dynamic mode (i.e., with an oscillating cantilever) allows the study of more sensitive sample surfaces and weakly adhering particles without damaging the structures or "cleaning up" the scanned area. Usually, surface modifications by means of a conventional SFM driven in dynamic mode are realized by switching off the feedback loop.[11−13] In this case, however, nonuniform results might occur because of the sample tilt and surface roughness. To avoid such effects, we have successfully induced surface modifications by increasing the amplitude of the dither piezo that drives the cantilever oscillations while the feedback loop has been continuously working.[8,10] This gives us the possibility to perform very precise and controlled manipulation experiments independent of the size of the modified surface area or the specific sample corrugations.

The use of colloidal latex spheres to produce closed-packed monolayers by self-assembly of submicron-sized particles is well-known. These colloidal arrays have been utilized as masks for metal evaporation to form periodic patterns on the micrometer or nanometer scale.[14,15] Here, latex spheres randomly deposited on graphite surfaces have served as a model system for demonstrating the controlled application of the DSM technique.

2. Experimental Section

Colloidal solutions of latex spheres (polystyrene latex) with radii from 50 to 110 nm in distilled water (1×10^{11} particles/mL) have been used for sample preparation (PLANO W. Plannet

* Corresponding author. Telephone: +49-30-2093-5549. Fax: +49-30-2093-5559. E-mail: claudia.ritter@epost.de.
† Humboldt-University Berlin.
‡ University of California at Berkeley.
§ Yale University.

(1) Quate, C. F. *Surf. Sci.* **1997**, *386*, 259−264.
(2) Sincell, M. *Science* **2000**, *290*, 1530.
(3) Jung, T. A.; Moser, A.; Hug, H. J.; Brodbeck, D.; Hofer, R.; Hidber, H. R.; Schwarz, U. D. *Ultramicroscopy* **1992**, *42−44*, 1446−1451.
(4) Miyake, S. *Appl. Phys. Lett.* **1995**. *67*, 2925−2927.
(5) Wendel, M.; Kühn, S.; Lorenz, H.; Kotthaus, J. P.; Holland, M. *Appl. Phys. Lett.* **1994**, *65*, 1775−1777.
(6) Klehn, B.; Kunze, U. *J. Appl. Phys.* **1999**, *85*, 3897−3903.
(7) Skaberna, S.; Versen, M.; Klehn, B.; Kunze, U.; Reuter, D.; Wieck, A. D. *Ultramicroscopy* **2000**, *82*, 153−157.
(8) Heyde, M.; Rademann, K.; Cappella, B.; Geuss, M.; Sturm, H.; Spangenberg, T.; Niehus, H. *Rev. Sci. Instrum.* **2001**, *72*, 136−141.
(9) Ramachandran, T. R.; Baur, C.; Bugacov, A.; Madhukar, A.; Koel, B. E.; Requicha, A. A. G.; Gazen, C. *Nanotechnology* **1998**, *9*, 237−245.
(10) Heyde, M.; Cappella, B.; Sturm, H.; Ritter, C.; Rademann, K. *Surf. Sci.* **2001**, *476*, 54−62.
(11) Junno, T.; Deppert, K.; Montelius, L.; Samuelson, L. *Appl. Phys. Lett.* **1995**, *66*, 3627−3629.
(12) Resch, R.; Baur, C.; Bugacov, A.; Koel, B. E.; Madhukar, A.; Requicha, A. A. G.; Will, P. *Langmuir* **1998**, *14*, 6613−6616.
(13) Resch, R.; Bugacov, A.; Baur, C.; Koel, B. E.; Madhukar, A.; Requicha, A. A. G.; Will, P. *Appl. Phys. A* **1998**, *67*, 265−271.
(14) Burmeister, F.; Schäfle, C.; Matthes, T.; Böhmisch, M.; Boneberg, J.; Leiderer, P. *Langmuir* **1997**, *13*, 2983−2987.
(15) Burmeister, F.; Badowsky, W.; Braun, T.; Wieprich, S.; Boneberg, J.; Leiderer, P. *Appl. Surf. Sci.* **1999**, *144−145*, 461−466.

10.1021/la011318n CCC: $22.00
Published on Web 09/11/2002

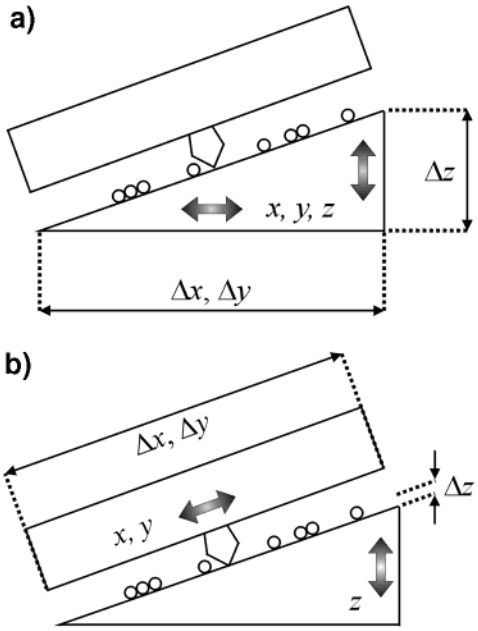

Figure 1. Schematic drawings depicting the benefits of a separation of the *x*−*y*-scan movement from the *z*-direction. A conventional combined *x*−*y*−*z*-scanner is shown in part a. Assuming a slight sample tilt of 3°, already more than 1 μm of *z*-movement is needed to follow the height profile of the surface within a 20-μm lateral translation. In contrast, the piezoelectric scan elements responsible for the lateral motion are aligned to the sample tilt in part b, which reflects the arrangement implemented in our present system. This reduces the necessary motion of the *z*-scanner to the actual sample corrugations. The height error between the *z*-movement and the effective sample corrugation can be easily neglected for all realistic sample tilts (it is, e.g., as low as 0.1% for a sample tilt of 3°).

GmbH, Wetzlar, Germany). A droplet of each of these solutions has been placed on freshly cleaved highly oriented pyrolytic graphite (HOPG) and dried in air.[16,17]

All experiments have been carried out with a home-built SFM, whose basic components have been reported in a previous article.[8] The experiments described here were performed with an advanced system. For example, the mechanical contact between the dither piezo and the cantilever chip was improved within the design of a new measuring head, and a higher mechanical stiffness of the system components has been obtained. This leads to a reduced drift of the system, resulting in a higher reproducibility of the scanning area (≤2 nm).

Another change is related to the scanning system. In common designs of SFMs, the scanner units (both scanning tip or scanning sample setups) are usually realized by a tripod or tube piezo, where a combined three-dimensional movement (*x*, *y*, *z*) can be achieved (see Figure 1a).[18] In contrast, we have implemented a separation of the scanning in the *x*−*y*-direction and the positioning in the *z*-direction by combining a piezoelectric scanning table for *x*−*y*-scanning and an independent *z*-piezo (Figure 1b). This allows a compensation of an eventual tilt of the sample surface with respect to the plane orthogonal to the *z*-direction (see the caption of Figure 1 for more details). Consequently, a higher digital resolution of the surface corrugation can be obtained even on long scan ranges. Moreover, the compensated sample tilt gives us the possibility to choose higher feedback parameters, which on the other hand may lead to a higher image quality. Both the scanning table for *x*−*y*-scanning and the *z*-piezo are equipped with integrated capacitive displacement sensors, to suppress nonlinearities (<0.03%) or hysteresis. Such a hardware-linearized scan control is essential for successful nanomanipulation experiments, since it enables precise positioning and motion of the tip with respect to the sample surface.

Commercially available cantilevers (Pointprobe NCL-50, Nanosensors, Aidlingen, Germany) with resonance frequencies $f = 170-190$ kHz and spring constants $c = 31-71$ N/m have been used to operate the SFM under ambient conditions in the dynamic mode (tapping mode with constant oscillation amplitude). The manipulation of the latex spheres has been carried out by increasing the amplitude V_{mod} of the oscillating voltage applied to the dither piezo that drives the cantilever vibrations. If the set-point amplitude chosen for the imaging mode is maintained (i.e., the feedback loop keeps the effective oscillation amplitude of the tip measured by the deflection sensor actively constant), an increased energy dissipation occurs when the tip touches the sample surface. Thus, by changing V_{mod}, it is possible to switch between an imaging mode and a manipulation mode with more or less energy transfer between tip and sample. Thereby, the active feedback during manipulation ensures a steady result independent of the sample tilt or topography changes.

3. Results and Discussion

The series of SFM images presented in Figure 2 illustrates the controlled manipulation of latex spheres by means of a vector-based manipulation procedure described below in more detail. The experiment demonstrates how different types of manipulations can be performed directly. Generally, any particle within the scanned surface area can be chosen for manipulation. The direction of the manipulation (translation or in-plane rotation) can be exactly assigned because of the high repositioning accuracy of our SFM.

For convenient observation of the performed manipulations, a two-particle assembly has been chosen for most of the manipulation experiments displayed in Figure 2. The image size is 1.2 μm × 1.2 μm, and the radii of individual latex spheres have been determined to be typically 50−60 nm. A white circle marks always the same sphere of the manipulated two-particle assembly. Each arrow in the images indicates the starting point, the direction, and the end of the path of the tip completed in DSM mode (i.e., with an applied V_{mod} large enough to induce particle displacements) between the before (continuous arrow) and the after (dashed arrow) movement image. Accordingly, the following image represents the result of the preceding manipulation step. The manipulation vectors were readily defined and mouse-controlled in a special user interface of our software. We find that the resulting movement of the assembly depends on where the two-particle assembly is pushed by the AFM tip. In Figure 2a, for example, the assembly was attacked at the lower sphere from the left side to the right. Figure 2b reveals that this lead to an in-plane rotation. A single latex sphere (marked by the square box) has its position near the manipulated two-particle assembly and would at a certain point disturb the next manipulation step. Therefore, the disturbing latex sphere has been pushed out of the relevant area (performed between images e and f), and manipulation of the two-particle assembly has been subsequently resumed.

The assembly of a specific nanostructure is demonstrated in Figure 3. Here, the letters "H" and "U" were formed from virtual disorder using the vector-based manipulation procedure, with parts a−c reflecting different stages of the formation process.

The DSM technique allows us not only to arrange nanoparticles in interesting patterns but also to gain information on the friction, deformation, adhesion, and cohesion of these particles. For example, it is reasonable to assume that the cohesion between the particles is larger

(16) Denkov, N. D.; Velev, O. D.; Kralchevsky, P. A.; Ivanov, I. B.; Yoshimura, H.; Nagayama, K. *Langmuir* **1992**, *8*, 3183−3190.
(17) Micheletto, R.; Fukuda, H.; Ohtsu, M. *Langmuir* **1995**, *11*, 3333−3336.
(18) Heyde, M.; Sturm, H.; Rademann, K. *Surf. Interface Anal.* **1999**, *27*, 291−295.

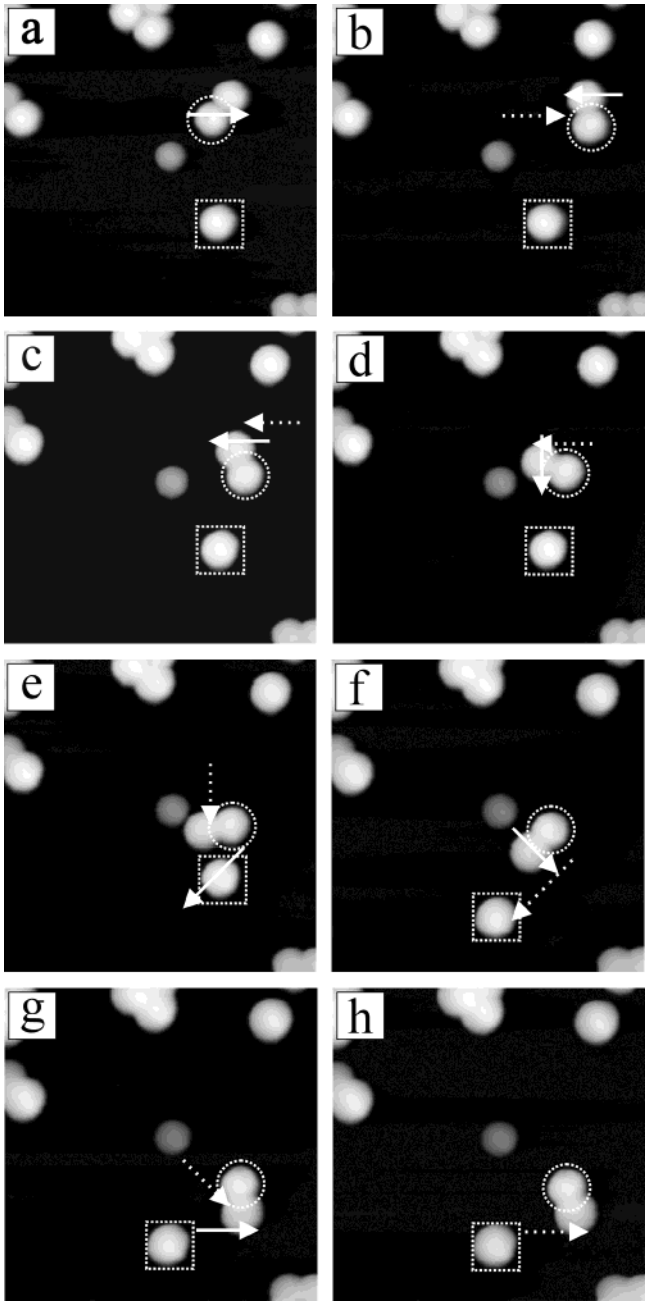

Figure 2. Direct, controlled translation and in-plane rotation of latex spheres using a vector-based user interface (scan range 1.2 μm × 1.2 μm, radii of latex spheres generally between 50 and 60 nm). The arrows indicate the path of the tip during manipulation carried out between the before (solid arrows) and the after (dashed arrows) movement image. The white circle and square, respectively, mark always the same latex spheres for convenient distinction of the individual manipulation steps.

than the adhesion to the substrate, since we were able to move the two-particle assembly featured in Figure 2 as an entirety. Nevertheless, a similar two-particle assembly could be divided into the two original latex spheres using a 10 times higher V_{mod} than that for the simple translation mode.

The experiment described in Figure 4 has been designed to study the frictional properties of the latex spheres. The idea behind this experiment is that the minimal value of V_{mod} needed to displace a sphere is proportional to the frictional force experienced during dislocation. To determine the corresponding threshold value of V_{mod}, a specific mask has been defined that controls the actual value of

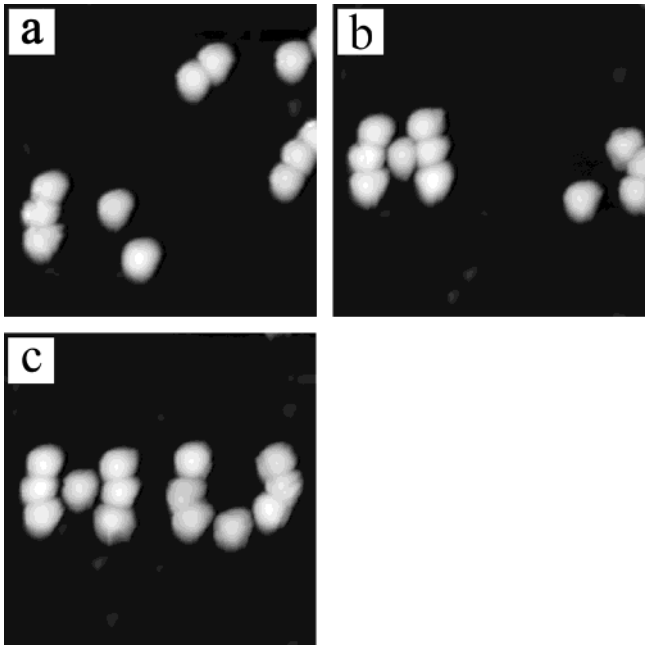

Figure 3. Formation of the letters "H" and "U" (for Humboldt University) as an example of a purposely designed two-dimensional nanostructure using the vector-based manipulation procedure introduced in Figure 2. Parts a−c illustrate different steps of the assembly process. The image size is always 2 μm × 2 μm; the radii of the individual latex spheres varied between 80 and 100 nm.

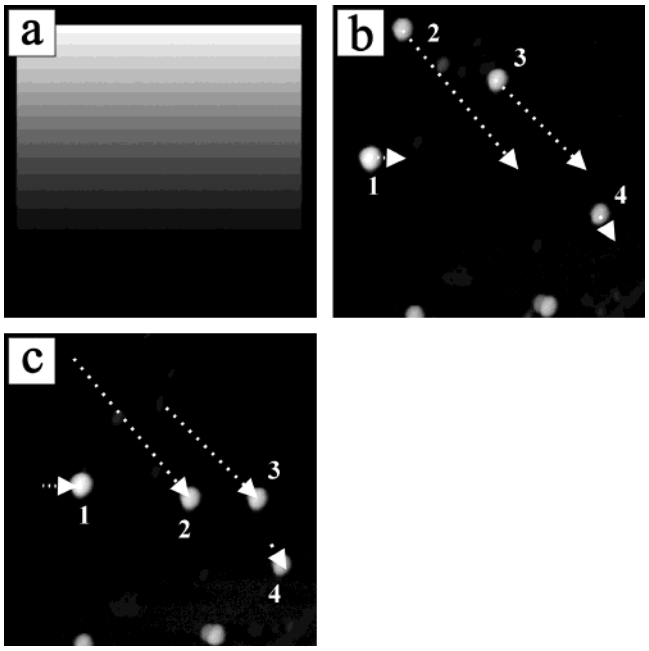

Figure 4. Manipulation experiment performed to find the threshold value of V_{mod} necessary to move the latex sphere. Image a reflects the definition of the pixel mask that determines the spot-dependent value of V_{mod} during manipulation (see text for details). The black frame prevents particles from being moved out of the sight of view. Images b and c show the topography of the scanned surface area (scan range 4 μm × 4 μm) before (b) and after (c) the mask defined in image a has been applied. Under the influence of the tip, the latex spheres marked with the numbers 1−4 have been displaced along the paths indicated by the dashed white arrows. The heights of the spheres are 215 nm (particle 1), 190 nm (particle 2), 185 nm (particle 3), and 165 nm (particle 4), respectively.

V_{mod} at each point of the scan area (see Figure 4a). In this mask, the value of V_{mod} is color-coded for each pixel of the

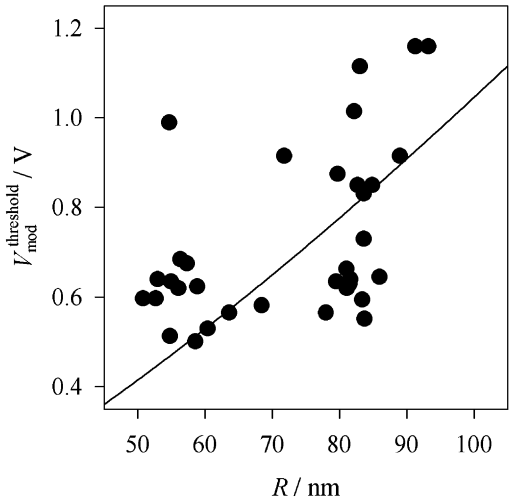

Figure 5. Plot of the threshold value of V_{mod} needed to displace latex spheres on the HOPG substrate surface as a function of the radius, R, for 38 particles. As a general trend, we find that larger spheres exhibit higher values of $V_{mod}^{threshold}$. The solid line represents the fit according to the relation $V_{mod}^{threshold} \propto R^{4/3}$ established in eq 7.

resulting image with bright colors representing high amplitudes and dark colors reflecting low amplitudes. The black frame of very low V_{mod} has been introduced to prevent spheres from being pushed out of the imaged area. The modifying mask is only applied while scanning from left to right (fast scan axis); the backward scan from right to left is performed with a value of V_{mod} low enough to prevent additional particle displacements. The slow scan axis is from top to bottom.

Parts b and c of Figure 4 display the topography of a surface area before and after, respectively, it has been modified utilizing the procedure described earlier. Particles within the inner mask area (i.e., within the black outer frame) are generally moved out of the path of the tip at an angle of about 45° (white arrows). As a consequence, the latex spheres advance every scan line somewhat more toward the lower right corner until V_{mod} falls below the threshold value for displacement. The experience from manipulation experiments such as the ones described in Figures 2 and 3 helped us to find appropriate maximum and minimum values for V_{mod}. By comparing the number of the scan line where the particle stopped (from Figure 4c) with the corresponding value of V_{mod} defined in the Figure 4a pixel mask, we could determine the threshold value for V_{mod}.

Two issues are worth noting from Figure 4. First, the particle labeled 1 only moved somewhat sideward, but not downward. It thus seems that the initial value needed to overcome friction for the first time is very close to (if not identical with) the threshold value of V_{mod} where motion stops. This is not trivial, since it could be suspected that residuals of the drying process might hinder the initial sphere motion. Second, we find roughly that spheres featuring smaller heights have lower associated threshold values of V_{mod}.

To investigate the last point more carefully, we plotted the threshold values of V_{mod} for 38 individual latex spheres as a function of their radii (see Figure 5). The sphere radii have been determined according to the procedure described in Figure 6. Despite a quite significant scatter of the individual data points, we tentatively can confirm the general trend observed that larger particles exhibit a higher threshold value of V_{mod}.

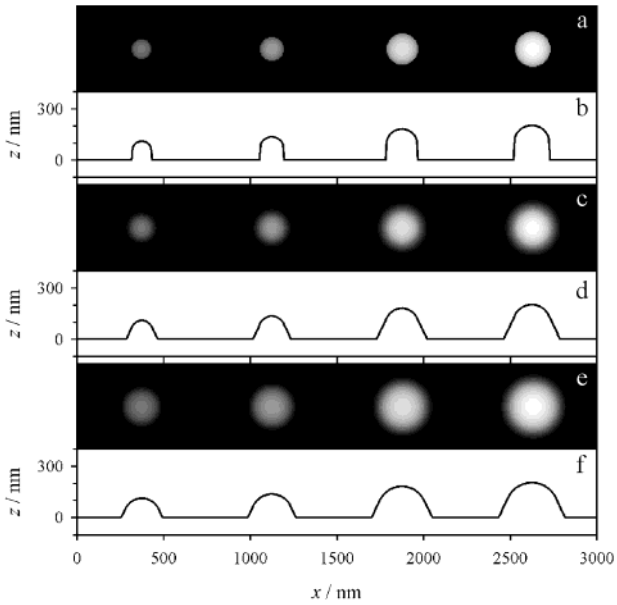

Figure 6. Series of figures illustrating the obstacles that have to be kept in mind while determining sphere radii from topographical SFM data. It shows three simulated images and the corresponding height profiles for four latex spheres with radii of 56, 68, 91, and 102 nm, respectively. Image size in parts a, c, and e is always 3000 nm × 500 nm. Three different types of tips have been used for the simulation: (a) ideal tip (assumed as a delta peak), (c) conical tip with 6-nm apex radius and 50° total opening angle, and (e) tip with 50-nm apex radius and 50° total opening angle. The corresponding height profiles across the centers of the spheres are displayed in parts b, d, and f, respectively. The influence of the tip geometry on the measured topography of the latex spheres (especially its apparent width) is clearly visible. This problem of tip convolution is well-known (see, e.g., refs 37−39). To circumvent this type of problem, we used half of the measured height of the particles as a true measure for the sphere radius. Note that the height can be very accurately quantified with an error of typically about 2 nm or less due to the capacitive hardware linearization of the z-piezomodule.[40]

As a prerequisite for an in-depth analysis, let us first recall recent experimental findings in the field of nanotribology. According to these findings, friction on the nanometer scale seems to be proportional to the contact area, A (see, e.g., refs 19 and 20 for recent reviews). The frictional force, F_f, may then be described by

$$F_f = \tau A \qquad (1)$$

where the proportional constant τ, the so-called shear strength, is the same for every latex sphere. As a consequence, the force needed to displace a latex sphere is supposably proportional to the a priori unknown contact area, A, of the latex sphere/substrate contact. An illustration of such a deformable sphere/substrate contact is displayed in Figure 7. Continuum elasticity theories describing the contact mechanics between a sphere and a flat surface are well developed;[21−26] however, most of

(19) Carpick, R. W.; Salmeron, M. *Chem. Rev.* **1997**, *97*, 1163−1197.
(20) Schwarz, U. D.; Hölscher, H. In *Modern Tribology Handbook;* Bhushan, B., Ed.; CRC Press: Boca Raton, FL, 2001; Vol. 1, pp 641−665.
(21) Johnson, K. L.; Kendall, K.; Roberts, A. D. *Proc. R. Soc. London, Ser. A* **1971**, *324*, 301−313.
(22) Derjaguin, B. V.; Muller, V. M.; Toporov, Y. P. *J. Colloid Interface Sci.* **1975**, *53*, 314−326.
(23) Muller, V. M.; Yushchenko, V. S.; Derjaguin, B. V. *J. Colloid Interface Sci.* **1980**, *77*, 91−101.
(24) Muller, V. M.; Yushchenko, V. S.; Derjaguin, B. V. *J. Colloid Interface Sci.* **1983**, *92*, 92−101.

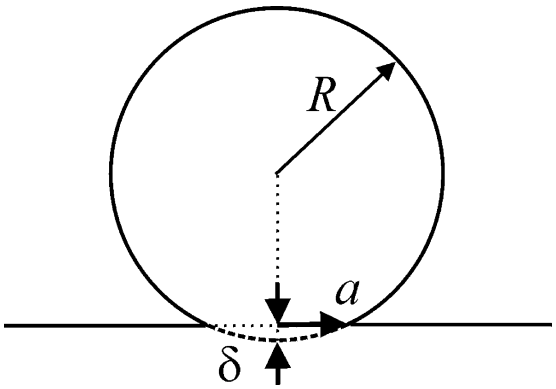

Figure 7. Sketch of an elastically deformable contact between a sphere and a flat surface. R denotes the radius of the sphere, a the radius of the contact area, and δ the deformation in the z-direction.

them require numerical solutions using a computer. For the sake of simplicity, we will restrict ourselves to an analysis of the problem in terms of simple analytical models.

Analytical theories for deformable spheres considering adhesion were presented by Johnson, Kendall, and Roberts[21] in 1971 (denoted as JKR theory in the following) and by Maugis in 1992[25] in an approximation of an earlier theory of Derjaguin, Muller, and Toporov[22] (the DMT-M or Hertz-plus-offset theory). Tabor[27] in 1977 has shown that the JKR theory applies if the parameter

$$\mu \equiv \left(\frac{16R\gamma^2}{9K^2z_0^3}\right)^{1/3} \qquad (2)$$

is large ($\mu \geq 5$) but the DMT-M theory applies if μ is small ($\mu \leq 0.1$).[28] Large values of μ indicate compliant contacts of large spheres, whereas small values imply hard contacts of spheres with small diameters. Here, R represents the radius of the sphere, γ is the work of adhesion, $K = {}^4/_3[(1 - \nu_1^2)/E_1 + (1 - \nu_2^2)/E_2]^{-1}$ reflects the reduced Young's modulus of the two surfaces (with $E_{1,2}$ and $\nu_{1,2}$ as Young's moduli and Poisson's ratios, respectively), while z_0 denotes their equilibrium spacing. In the intermediate regime, however, none of the theories apply, and one of the more complex theories requiring numerical solutions has to be applied.[23−26]

Assuming $E_{\mathrm{HOPG}} = 17$ GPa, $\nu_{\mathrm{HOPG}} = 0.3$, $E_{\mathrm{latex\ sphere}} = 3$ GPa, $\nu_{\mathrm{latex\ sphere}} = 0.34$, $\gamma = 50$ mJ/m^2 (typical value for van der Waals surfaces), $z_0 = 3$ Å, and $R = 50-110$ nm, we find a parameter μ for our system of about 0.8−1.0, which is well within the intermediate regime. As a consequence, a correct analytical description of the present sphere/flat contact is not possible. In the following discussion, we will therefore consider both the JKR and the DMT-M models.

The contact area−load dependence within the JKR model is given by[21,29]

$$A_{\mathrm{JKR}} = \pi\left(\frac{R}{K}\right)^{2/3}\left(\sqrt{F_l - F_c^{\mathrm{JKR}}} + \sqrt{-F_c^{\mathrm{JKR}}}\right)^{4/3} \qquad (3)$$

Here, F_l is the externally applied loading force, and $F_c^{\mathrm{JKR}} = -1.5\pi R\gamma$ is the critical force needed to separate the sphere from the substrate. Since no external loading force is applied, F_l can be identified as the gravitational force $F_l = {}^4/_3\pi g\rho R^3$. Using 1050 kg/m^3 for the density of the polystyrene latex spheres, ρ, and a maximum radius of the spheres of 110 nm, we find a value of F_l in the range of 10^{-8} nN.

In contrast, the critical force has a value in the range of 10 nN for the same radius of the sphere with the assumption of a van der Waals surface ($\gamma \approx 50$ mJ/m^2).[30] This huge difference between F_c^{JKR} and F_l of 9 orders of magnitude allows us to neglect the value of the gravitational force and to rewrite eq 3 in the form[31]

$$A_{\mathrm{JKR}} = \pi\left(\frac{6\pi\gamma}{K}\right)^{2/3}R^{4/3} \propto R^{4/3} \qquad (4)$$

By introducing typical values for our latex spheres, we find A_{JKR} to be between 220 and 650 nm^2.

The equation to calculate the contact area within the DMT-M model is given by[25]

$$A_{\mathrm{DMT-M}} = \pi\left(\frac{R}{K}\right)^{2/3}(F_l - F_c^{\mathrm{DMT-M}})^{2/3} \qquad (5)$$

where $F_c^{\mathrm{DMT-M}} = -2\pi R\gamma$ reflects again the critical force.[22] The same line of arguments as that above leads then to

$$A_{\mathrm{DMT-M}} = \pi\left(\frac{2\pi\gamma}{K}\right)^{2/3}R^{4/3} \propto R^{4/3} \qquad (6)$$

Values calculated with the DMT-M model of $A_{\mathrm{DMT-M}}$ are between 100 and 320 nm^2 for $R = 50-110$ nm. That is, both models result in the same dependence of the effective contact area, A, on the sphere radius, R, of $A \propto R^{4/3}$. Considering eq 1 and our earlier assumption that the threshold value of V_{mod} is proportional to the frictional force, we find that $V_{\mathrm{mod}}^{\mathrm{threshold}}$ depends on the radii of the latex spheres, according to

$$V_{\mathrm{mod}}^{\mathrm{threshold}} \propto F_f \propto R^{4/3} \qquad (7)$$

A fit based on eq 7 has been included in Figure 5. Even though the scatter of the experimental data points prevents a positive proof of this or similar dependencies, the overall appearance nevertheless corroborates this model.

A significant drawback of eq 7 is that there is no evident route of how the proportional constant between $V_{\mathrm{mod}}^{\mathrm{threshold}}$ and F_f can be determined. To nevertheless obtain at least a rough estimate of an upper limit for F_f, we may make use of the relation between the theoretical shear stress, τ^{theo}, and the shear force modulus, $G = E/(2 + 2\nu)$,[32] of $\tau^{\mathrm{theo}} = G/30$.[33] Replacing G by the effective shear modulus of the contact, $G^* = [(2 - \nu_1)/G_1 + (2 - \nu_2)/G_2]^{-1}$,[34] yields a shear strength of $\tau^{\mathrm{theo}} \approx 19$ MPa, which is in the range of similar values given in the literature.[35,36] For contact areas of 100−650 nm^2, as determined earlier for the present case, this results in an upper limit for F_f of between 2 and 13 nN.

(25) Maugis, D. *J. Colloid Interface Sci.* **1992**, *150*, 243−269.
(26) Greenwood, J. A. *Proc. R. Soc. London, Ser. A* **1997**, *453*, 1277−1297.
(27) Tabor, D. *J. Colloid Interface Sci.* **1977**, *58*, 2−13.
(28) Johnson, K. L. *Tribol. Int.* **1998**, *31*, 413−418.
(29) Persson, B. N. J., Tosatti, E., Eds. *Physics of Sliding Friction;* Kluwer Academic Publishers: Dordrecht, The Netherlands, 1996.
(30) Israelachvili, J. N. *Intermolecular and Surface Forces*, 2nd ed.; Academic Press: San Diego, CA, 1991.
(31) Mahoney, W.; Schaefer, D. M.; Patil, A.; Andres, R. P.; Reifenberger, R. *Surf. Sci.* **1994**, *316*, 383−390.
(32) Timoshenko, S. P.; Goodier, J. N. *Theory of Elasticity*; McGraw-Hill Classic Textbook Reissue Series; McGraw-Hill: New York, 1987.
(33) Cottrell, A. H. *Dislocations and Plastic Flow in Crystals;* Oxford University Press: Oxford, U.K., 1953.
(34) Lantz, M. A.; O'Shea, S. J.; Welland, M. E.; Johnson, K. L. *Phys. Rev. B* **1997**, *55*, 10776−10785.

Finally, a last issue should be noted in this context. In our earlier discussions, we always considered the spheres to slide over the surface. However, a sphere undergoing lateral motion while in contact with a surface can either *slide* or *roll*. At the macroscopic scale, rolling is generally preferred over sliding. To exclude rolling as the preferred type of motion in our experimental system, we used the DSM technique to mark a single latex sphere with a light dent (see Figure 8a). The marked latex sphere has subsequently been moved over a distance of 250 nm using the vector-oriented manipulation procedure introduced in Figure 2. Thereby, a V_{mod} sufficient for particle translation, but low enough to prevent any further plastic deformation of the sphere, has been applied. Figure 8b shows the result of the manipulation step. Comparison of parts a and b of Figure 8 as well as the corresponding insets displaying *z*-profiles taken along the dashed−dotted lines reveals that only a small in-plane rotation has occurred during particle dislocation caused by the somewhat off-centered point of attack during manipulation. This small in-plane rotation of about 13° gives evidence that the unsymmetrical profile is not caused by a tip convolution effect. On the other hand, the lateral translation of 250 nm was considerably smaller than the perimeter of the sphere of about 350 nm, ruling out the possibility of a full turn. Additionally, assemblies of latex spheres, as shown in Figure 2, have also been moved, and the experimental data indicate that the clusters have been slid rather than rolled.

4. Conclusions

In summary, we have demonstrated that, by means of the dynamic surface modification technique, a controlled lateral positioning and in-plane rotation of structurally unchanged nanometer-sized latex spheres can be performed reproducibly with high precision. In contrast to earlier reports of surface modifications applying a similar technique, both imaging mode and manipulation mode were operated with an active feedback loop to ensure uniform results of the modification steps independent of the sample tilt or surface corrugation. By choosing appropriate values for V_{mod} (representing the amplitude of the oscillating voltage applied to the dither piezo that drives the cantilever oscillations), we were allowed by the presented technique to easily switch among imaging, translation or in-plane rotation of nanoparticles, marking single nanoparticles, and cutting of nanoparticles.

Because of this flexibility, the manipulation technique was found to be suitable to study the adhesion, cohesion, and friction of nanoparticles adsorbed on surfaces. In such experiments, it has been demonstrated in particular that the motion of the particles occurs most likely in sliding rather than in rolling. The threshold amplitude of V_{mod} needed to overcome the static friction of a single latex sphere has been shown to be dependent on the size of the manipulated spheres. A $V_{mod}^{threshold} \propto R^{4/3}$ law has been established that is corroborated by the experimental data. However, a significant scatter of the experimental data, probably induced mainly by the undefined preparation conditions of the particle solutions and the sample in air, prevents a strict validation of the relation. Future tests should also include the variation of the radii within a much wider range than that used here.

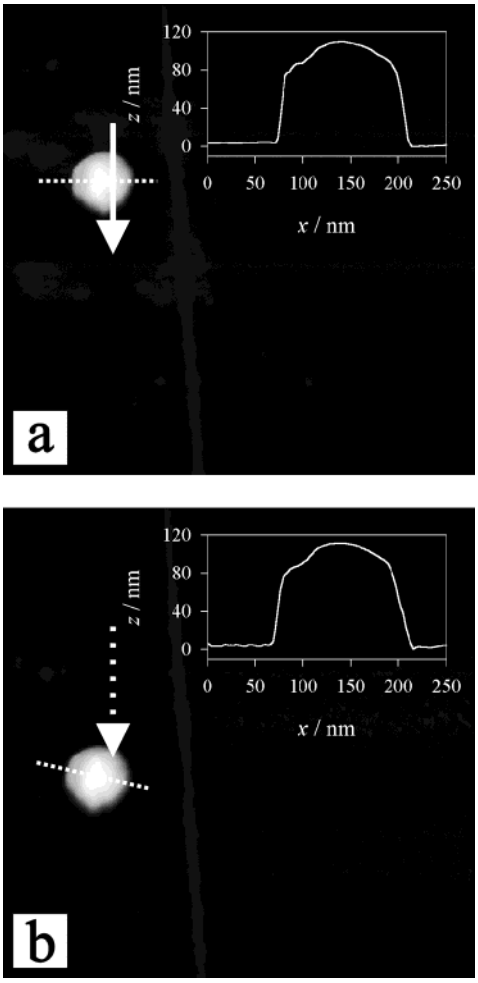

Figure 8. Purposely marked latex sphere (see text) before (a) and after (b) lateral translation (image size, 1 μm × 1 μm; height of the sphere, 110 nm). The white arrows reflect the path of the tip during manipulation. The dash−dotted lines indicate the direction along which the height profile shown in the inset has been taken. Since the sphere exhibits the same asymmetric profile before and after translation, a sliding motion is assumed.

Acknowledgment. Financial support from the Deutsche Forschungsgemeinschaft (Leibniz Prize (M.H., C.R., K.R.) and Grant No. 641/1-1 (U.S.)), the Department of Energy of the United States of America (Contract No. DE-AC03-76SF00098 (M.H., U.S.)), and the Feodor Lynen Fellowship of the Alexander von Humboldt Foundation (M.H.) is gratefully acknowledged.

LA011318N

(35) Meyer, E.; Overney, R.; Brodbeck, D.; Howald, L.; Lüthi, R.; Frommer, J.; Güntherodt, H.-J. *Phys. Rev. Lett.* **1992**, *69*, 1777−1780.
(36) Sheehan, P. E.; Lieber, C. M. *Science* **1996**, *272*, 1158−1161.
(37) Schwarz, U. D.; Haefke, H.; Reimann, P.; Güntherodt, H. J. *J. Microsc. (Oxford)* **1994**, *173*, 183−197.
(38) Odin, C.; Aime, J. P.; El Kaakour, Z.; Bouhacina, T. *Surf. Sci.* **1994**, *317*, 321−340.
(39) Villarrubia, J. S. *J. Res. Nat. Inst. Stand. Technol.* **1997**, *102*, 425−454.
(40) For an absolutely exact determination of the sphere radii, elastic deformation under the influence of attractive adhesive forces would need to be considered, noting that the measured height of a latex sphere is slightly below the "real" diameter of the free sphere.[31] This difference, however, is very small. For instance, no upsetting was visible in scanning electron microscopy images of similarly prepared samples.[41] Alternatively, the deformation can be also calculated within the Johnson, Kendall, and Roberts or Maugis' approximation of the Derjaguin, Muller, and Toporov theory, introduced below. Following these models, we calculated deformations δ of 0.5−0.9 nm, assuming typical values as those given later in the text. A maximum deformation of about 0.9 nm exhibited by a latex sphere with a diameter of 220 nm is less than 0.4%; therefore, this effect is neglected in the following.
(41) S. Rogaschewski (Humboldt University Berlin, Institute of Physics), private communication.